

Article

Numerical Modelling for Synthetic Fibre Mooring Lines Taking Elongation and Contraction into Account

Ivan Čatipović *, Neven Alujević, Smiljko Rudan  and Vedran Slapničar * 

Faculty of Mechanical Engineering and Naval Architecture, University of Zagreb, Ivana Lučića 5, 10000 Zagreb, Croatia; neven.alujevic@fsb.hr (N.A.); smiljko.rudan@fsb.hr (S.R.)

* Correspondence: ivan.catipovic@fsb.hr (I.Č.); vedran.slapnicar@fsb.hr (V.S.)

Abstract: Synthetic fibre mooring lines are used as an alternative to traditional steel wire ropes due to their higher strength to weight ratio. Benefits are also found in relative ease of handling, and therefore the marine industry has largely accepted this type of mooring line. By rules and regulations, the design of mooring lines should be based on a coupled dynamic analysis of a particular mooring system and moored vessel. This approach incorporates damping and inertial forces (i.e., hydrodynamic reactions) acting directly on the mooring lines due to their motion through the seawater. On the basis of the outer diameter of the synthetic fibre rope, the Morison equation gives estimations of the mooring line hydrodynamic reactions. In comparison to the traditional steel wire ropes, the synthetic mooring lines usually have relatively larger elongations and consequently larger reductions of the outer diameter. Furthermore, the lower diameter certainly leads to reduced values of damping and added mass (of mooring lines) that should be considered in the coupled model. Therefore, the aim of this study was to develop a new numerical model that includes diameter changes and axial deformations when estimating the hydrodynamic reactions. The development of the model is carried out with a nonlinear finite element method for mooring lines with the assumption of large three-dimensional motions. The obtained results show the effectiveness of the newly developed model as a more accurate approach in calculation of hydrodynamic reactions.

Keywords: mooring lines; synthetic fibre ropes; damping; added mass; nonlinear finite element method



Citation: Čatipović, I.; Alujević, N.; Rudan, S.; Slapničar, V. Numerical Modelling for Synthetic Fibre Mooring Lines Taking Elongation and Contraction into Account. *J. Mar. Sci. Eng.* **2021**, *9*, 417. <https://doi.org/10.3390/jmse9040417>

Academic Editor: Lars Bergdahl

Received: 16 March 2021

Accepted: 10 April 2021

Published: 13 April 2021

Publisher's Note: MDPI stays neutral with regard to jurisdictional claims in published maps and institutional affiliations.



Copyright: © 2021 by the authors. Licensee MDPI, Basel, Switzerland. This article is an open access article distributed under the terms and conditions of the Creative Commons Attribution (CC BY) license (<https://creativecommons.org/licenses/by/4.0/>).

1. Introduction

Synthetic fibre mooring lines are used as an alternative to traditional steel wire ropes and chains due to their lower submerged mass, lower cost, the potential to reduce peak loadings, and the reduced footprint of the floating systems [1]. It has been shown that the elastic synthetic rope has great potential in the application of wave energy converter (WEC) mooring system [2]. Moreover, the decommissioning process and reuse possibilities of synthetic ropes are being studied since this provides an opportunity for financial, environmental, and socioeconomic benefits [3,4].

Mooring-induced damping plays a significant role in limiting surge response of single-point moored ship-like platforms in survival conditions and thus in reducing the danger of mooring system failure [5]. As the water depth for offshore oil drilling increases, mooring lines are more and more often made of synthetic ropes [6]. Damping qualities of such lines regarding slow-drift oscillations are critical when designing spread-mooring systems. The dynamic effects of mooring lines can significantly reduce the low-frequency resonant responses of the system motions [7].

Tests on a ship model with catenary mooring showed that the mooring-induced damping contribute to about 80% of the total damping [8]. Moreover, the superposition of the first-order excitation on the slowly varying second-order excitation increases the damping by a factor in the range of 2–4. Full-scale decay test made with a tanker confirmed that the damping is of viscous type and that theoretical models are able to recover roughly

75% of the observed damping while the energy dissipation in the mooring lines is the major part [9].

Physical model tests of moored vessels with full depth mooring system are not possible because no tank facility is sufficiently large enough to perform the model testing intended for large seawater depths with an acceptable model scale. Therefore, model tests with truncated mooring system have been developed. The similarity with the full-depth mooring system can be achieved through an optimisation of the parameters of truncated mooring line with consideration of the static and damping characteristics [10]. The truncation approaches that include mooring lines' inertial forces have also been developed and are used for the catenary, semi-taut, and taut mooring systems in both extreme and working wave conditions [11,12].

The drag-induced damping of a mooring cable due to the combined first- and second-order wave-excited motion of a moored vessel can be determined by statistical linearisation [13]. A significant influence of the mooring line damping on the response amplitude operators (RAOs) for all the degrees of freedom is found to be especially important at higher seas. The effects on the mooring line damping considering different random motions of a moored vessel are found to be irregular [14]. The amplification of the mooring damping comes with the increase of the significant wave height and zero crossing period, but the RAOs play a dominant role in determining the amplification factor. In order to study the mooring damping in real sea states, one can apply a novel de-coupled technique [15]. The results of this technique indicate that the mooring tensions and the induced damping are closely related.

The superposition of the wave frequency motion on the low-frequency motion of a moored vessel significantly amplifies the damping induced by the mooring lines [16]. A possible reason for this is the proportionality of the drag force to the square of the velocity. For a taut mooring line, small increases in the motion speed and amplitude at the fairlead would cause a considerable increase in the drag force on the entire line, resulting in a significant increase of the damping. Simple approximate expressions for taut mooring lines are developed in [17] for the maximum tension as well as mooring line damping under the assumption that the tension in the line is large relative to the submerged weight of the line. Coupled dynamic analyses conducted for various polyester segment diameters have shown a reduction of the surge response corresponding to the increase in mooring line diameter [18].

The design of a mooring system for WECs must consider reliability, survivability, and an efficient energy conversion. For catenary moored WECs, the damping properties of mooring lines are increased by their stiffness characteristics and thus lead to an accumulated cyclic loading of the overall mooring system. In particular, the fatigue damage could become a major source of failure for such installations [19]. Within wave-wind-induced dynamic analyses of a floating wind turbine (FWT), the wave frequency part of the tension response is not affected by the mooring line hydrodynamic damping [20]. However, the tension response associated to the yaw resonant motion and eigenfrequencies of the lines are significantly affected by the mooring line hydrodynamic damping.

The usual dynamic mooring analysis only considers hydrodynamic forces over the mooring line induced by the relative motion of the line through the still seawater. With such an approach, the direct wave loads acting on a mooring line are disregarded. The International Energy Agency (IEA) Wind Task 30 extension proposal identifies the importance for a future investigation of wave forces on floating offshore wind turbine (FOWT) mooring lines [21]. In line with the proposal, a catenary moored FOWT was studied, and it was found that the inclusion of direct wave loads led to 5% increase of the fatigue damage in the most loaded line [22]. In this study, the water particle acceleration and the water particle velocity due to the incoming waves were accounted for, i.e., the inertial and drag part of the direct wave loads were included. For an underwater floating structure with moorings, the magnitudes of the wave forces acting on the mooring lines could reach up to 12% of the incident wave forces [23].

Studies on coupled models clearly bring out the importance of hydrodynamic damping from moorings on traditional offshore structures [24,25] as well as on offshore renewables [26,27] and on marine aquaculture structures [28]. The assumption of the nonlinear drag model as a quadratic function of relative velocity between the water particle and structure as well as the drag force coefficient used are both empirically defined. Forces on moorings (and risers) that oscillate/vibrate are generally evaluated using the well-known generalised Morison equation [29,30].

In the current practice, there are many existing methods for describing mooring lines. The lumped mass method is currently widely used in the mooring dynamic analysis, e.g., for modelling of a multi-component mooring line [31] or to study the tensions of a mooring line with an embedded segment at an ultra-deepwater location [32]. This model is applicable for the implementation of the mooring line damping by Morison equation [16]. Furthermore, this model can be coupled with the smoothed particle hydrodynamics (SPH) as a more advanced and reliable approach to study the fluid–structure interaction [33,34].

The mooring system dynamics can be calculated by the finite differences method, which accounts for the mooring lines' physical characteristics such as mass and stiffness as well as for the hydrodynamic inertial and damping characteristics [35]. The interaction of the mooring lines with the seabed can be considered along with the bending and the torsional stiffness of used cables [36]. This was particularly important in the recent studies of the offshore renewables.

The finite element model can be developed by the principle of virtual work to obtain discrete equations for numerical computation. Due to high nonlinearity of the discrete motion equations of mooring lines, usually some incremental and iterative schemes are applied in the solution procedures [37]. The Morison equation is used to calculate the hydrodynamic forces. This model is very versatile, and recently is used for some studies found in practical problems as an investigation of the interaction between ship generated waves and slender structures [38] or for the position keeping of a crane barge during use [39]. Furthermore, this model is effectively coupled with the hydro-elastic model of a floating body in regular and irregular waves [40] and with the motions of a remotely operated vehicle (ROV) to assess its efficiency and safety [41,42].

Synthetic mooring lines usually have relatively large elongations, even when made of novel types of rope [25,43]. Since Poisson's ratio for synthetic ropes can be assumed as 0.5 [44], a significant reduction of the outer rope diameter can be expected. By Morison equation, the reduced diameter will lead to reduced values of the damping and the added mass of such mooring lines, i.e., to reduced values of the hydrodynamic reactions. This reduction of damping and added mass has not yet been considered in the literature. The methods for describing mooring lines (the lumped mass method, the finite difference method, the finite element method) evaluates the damping and the added mass on the basis of the initial value of the mooring line diameter, i.e., considering it to be constant. The influence of the axial deformation, in the listed methods, is considered with regard to evaluations of the stiffness forces and the displacements but not in terms of evaluations of the damping and the added mass (as the hydrodynamic reactions). The influence of the axial deformation on the diameter is left out and, consequently, the axial deformation is neglected when the damping and the added are evaluated. This is also the case in some analytical (catenary) approaches used in the current practice [45], as well as in some special methods such as the harmonic balance method [46] and an advanced finite element method [47].

Therefore, the principal aim of this study was to develop a new numerical model that considers the diameter change when estimating the hydrodynamic reactions. The elongation of the mooring line was considered as well. To illustrate the effectiveness of the newly developed model, we observed simple mooring line segments made of a synthetic rope, i.e., a straight segment and a curved segment. These simplified set-ups enabled the development of formulations of exact analytical expressions for the damping and the added mass. Since there are no available experimental results that are focused on this issue

in detail, the analytical expressions were used as an independent numerical validation of the proposed model and to present the improvement over the current practice.

2. Mathematical Model

The influence of the relatively large elongations of mooring lines on its stiffness is studied in [48], where a Taylor series expansion of the expression containing the axial deformation was used. The effectiveness of this approach was presented within motion calculations of a floating production storage and offloading (FPSO) unit [49]. A similar study considering offshore renewables was carried out in [50]. The approach with the Taylor series expansion is adopted hereafter.

2.1. Loads on Mooring Line

The deformed shape of a mooring line is described by a spatial curve. In the governing equations, the spatial curve is defined by a position vector \mathbf{r} in the global coordinate system $Oxyz$ (see Figure 1). A point on the curve is defined by an arc length \tilde{s} of the extended mooring line. Within the dynamic analysis, the position vector \mathbf{r} is dependent on the time variable t . An equivalent segment of the mooring line is set according to the approach on the basis of the effective tension and the effective load [51,52]. This approach is developed in order to include the influence of the outer hydrostatic pressure due to the seawater on the mooring line. The segment of the mooring line is shown in Figure 1.

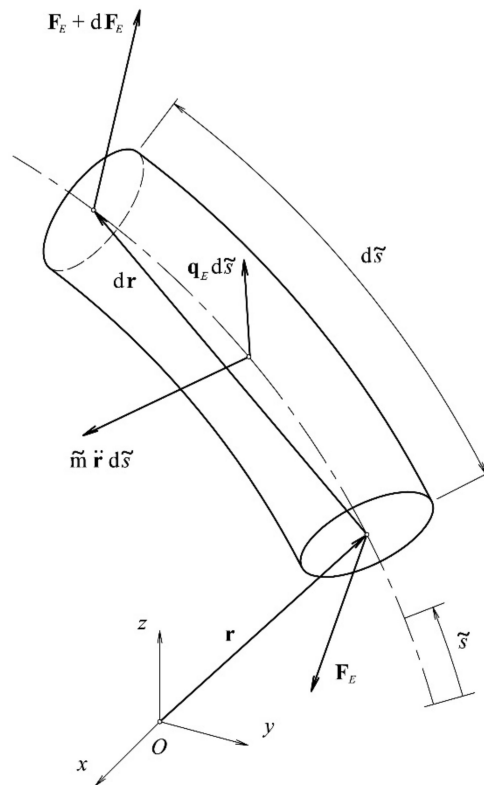


Figure 1. The segment of the mooring line [48].

The vector of the effective load \mathbf{q}_E contains buoyancy \mathbf{q}_B , weight of the mooring line \mathbf{q}_W (i.e., dry weight), and hydrodynamic loads \mathbf{q}_H

$$\mathbf{q}_E = \mathbf{q}_B + \mathbf{q}_W + \mathbf{q}_H \tag{1}$$

The loads are distributed along the extended length of the segment $\tilde{d}s$. The buoyancy and the weight are defined simply as

$$\mathbf{q}_W = \tilde{m} \mathbf{g} \tag{2}$$

$$\mathbf{q}_B = -\rho \tilde{A} \mathbf{g} \tag{3}$$

where \tilde{m} is the mass per unit length of the segment. Density of the seawater is denoted as ρ , while \mathbf{g} is the gravity acceleration vector pointing in the opposite direction of the z-axis of the global coordinate system. Cross-sectional area of the segment is given by \tilde{A} .

The inertial load due to the own mass of the segment is also considered in this model. The vector $\ddot{\mathbf{r}}$ denotes the acceleration of the segments (since $\dot{\mathbf{r}}$ represents the second derivative with respect to time), and therefore the term $\tilde{m} \ddot{\mathbf{r}} d\tilde{s}$ in Figure 1 is the inertial load.

The segment of the mooring line is extended to the length $\tilde{d}s$ due to the applied loads. The strain ϵ , being an axial deformation, is defined as

$$\epsilon = \frac{d\tilde{s} - ds}{ds} \tag{4}$$

where ds is length of the non-extended segment, i.e., the segment observed in the stress-free configuration of the mooring line. Therefore, the relation between $d\tilde{s}$ and ds is

$$d\tilde{s} = (1 + \epsilon)ds \tag{5}$$

Variables \tilde{m} and \tilde{A} in Equations (2) and (3) are related to the extended state of the segment and therefore are dependent on the axial deformation ϵ . Poisson’s ratio for synthetic ropes can be assumed as 0.5 [44]. For this particular value of Poisson’s ratio, the volume of a deformed segment is conserved. Due to this conservation principle, the distributed mass \tilde{m} and the cross-section area \tilde{A} can be defined as

$$\tilde{m} = \frac{m}{1 + \epsilon} \tag{6}$$

$$\tilde{A} = \frac{A}{1 + \epsilon} \tag{7}$$

where A and m are related to the non-extended state of the segment so that they can be defined as an input.

The hydrodynamic loads \mathbf{q}_H from Equation (1) are formulated by the Morison equation:

$$\mathbf{q}_H = -C_A \rho \tilde{A} \ddot{\mathbf{r}}^n + C_M \rho \tilde{A} \dot{\mathbf{v}}^n + \frac{1}{2} C_D \rho \tilde{D} \left\| \mathbf{v}^n - \dot{\mathbf{r}}^n \right\| \left(\mathbf{v}^n - \dot{\mathbf{r}}^n \right) \tag{8}$$

where $\| \cdot \|$ denotes vector modulus. C_A , C_M , and C_D are the added mass, the inertial coefficient, and drag coefficient, respectively. The cross-section area of the extended segment is denoted by \tilde{A} (as in the expression for the buoyancy). The diameter, which is elongation dependent, is given as \tilde{D} . By the same conservation principle used in Equation (7) for \tilde{A} , the relation for \tilde{D} can be formulated as

$$\tilde{D} = \frac{D}{\sqrt{1 + \epsilon}} \tag{9}$$

The Morison equation given by Equation (8) consists of 3 members. The first member is considered as the inertial force due to the acceleration of the segment through the still seawater. This term is used for the formulation of the added mass. The second member is

also a part of the inertial force but is caused by the flow acceleration of the seawater on the fixed segment. The third member is the drag force that is related to the relative velocity of the segment and the seawater flow. The third member is used for the formulation of the damping within the motion equation [29,30]. Thus, the drag force is the damping in considerations of the mooring line dynamics.

Vector $\ddot{\mathbf{r}}^n$ in Equation (8) is a component of the mooring line acceleration normal to the deformed mooring line

$$\ddot{\mathbf{r}}^n = \ddot{\mathbf{r}} - \left(\ddot{\mathbf{r}} \cdot \frac{d\mathbf{r}}{d\tilde{s}} \right) \frac{d\mathbf{r}}{d\tilde{s}} \tag{10}$$

where \cdot denotes a scalar product. The above equation is formulated on the basis of Figure 2. The second term on the right-hand side is the projection of the total acceleration $\ddot{\mathbf{r}}$ to the tangent $d\mathbf{r}/d\tilde{s}$ of the deformed and extended mooring line. The term $d\mathbf{r}/d\tilde{s}$ is the unit tangent vector by definition, and thus the second term on the right side is the tangential component of the acceleration. The normal acceleration component can be obtained by subtracting the acceleration tangential component from the total acceleration. In an analogue way, $\dot{\mathbf{r}}^n$ is defined as the normal component of the mooring line velocity. Furthermore, motion of surrounding seawater is considered through normal components of the water particle acceleration $\dot{\mathbf{v}}^n$ and velocity \mathbf{v}^n . These vectors are given by

$$\begin{aligned} \dot{\mathbf{r}}^n &= \dot{\mathbf{r}} - \left(\dot{\mathbf{r}} \cdot \frac{d\mathbf{r}}{d\tilde{s}} \right) \frac{d\mathbf{r}}{d\tilde{s}} \\ \mathbf{v}^n &= \mathbf{v} - \left(\mathbf{v} \cdot \frac{d\mathbf{r}}{d\tilde{s}} \right) \frac{d\mathbf{r}}{d\tilde{s}} \\ \dot{\mathbf{v}}^n &= \dot{\mathbf{v}} - \left(\dot{\mathbf{v}} \cdot \frac{d\mathbf{r}}{d\tilde{s}} \right) \frac{d\mathbf{r}}{d\tilde{s}} \end{aligned} \tag{11}$$

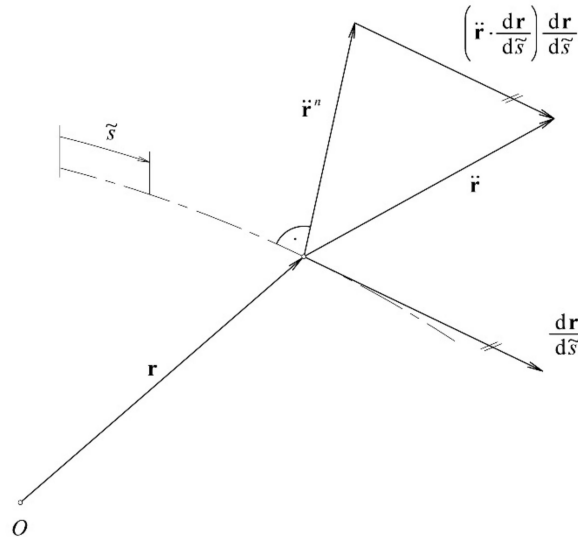


Figure 2. Normal component of the mooring line acceleration.

In the present model, the unit tangent vector is obtained by differentiation of the spatial curve \mathbf{r} with respect to the extended segment length as $d\mathbf{r}/d\tilde{s}$. This is in contrast to current practice where the unit tangent is evaluated on the basis of the non-extended segment length in the form $d\mathbf{r}/ds$, which is a poor approximation for synthetic fibre mooring lines. This is because, as already mentioned, synthetic mooring lines usually undergo a relatively large axial deformation ϵ and thus great differences in the extended $d\tilde{s}$ and the non-extended length ds exist, as given by Equation (5). Therefore, the model developed here has an advantage in calculating hydrodynamic loads since it incorporates a more accurate expression for tangential and normal components of velocities and accelerations.

Normal acceleration given in Equation (10) is now reformulated as

$$\ddot{\mathbf{r}}^n = \frac{d \mathbf{r}}{d \tilde{s}} \times \left(\ddot{\mathbf{r}} \times \frac{d \mathbf{r}}{d \tilde{s}} \right) \tag{12}$$

where \times denotes a vector product. The new form is obtained by the vector triple product, keeping in mind that $d \mathbf{r}/d \tilde{s}$ is a unit vector. In the same way, the expressions in Equation (11) can also be reformulated as

$$\begin{aligned} \dot{\mathbf{r}}^n &= \frac{d \mathbf{r}}{d \tilde{s}} \times \left(\dot{\mathbf{r}} \times \frac{d \mathbf{r}}{d \tilde{s}} \right) \\ \mathbf{v}^n &= \frac{d \mathbf{r}}{d \tilde{s}} \times \left(\mathbf{v} \times \frac{d \mathbf{r}}{d \tilde{s}} \right) \\ \dot{\mathbf{v}}^n &= \frac{d \mathbf{r}}{d \tilde{s}} \times \left(\dot{\mathbf{v}} \times \frac{d \mathbf{r}}{d \tilde{s}} \right) \end{aligned} \tag{13}$$

as well as a part of the last term in Equation (8)

$$\left\| \mathbf{v}^n - \dot{\mathbf{r}}^n \right\| \left(\mathbf{v}^n - \dot{\mathbf{r}}^n \right) = \left\| (\mathbf{v} - \dot{\mathbf{r}}) \times \frac{d \mathbf{r}}{d \tilde{s}} \right\| \left\{ \frac{d \mathbf{r}}{d \tilde{s}} \times \left[(\mathbf{v} - \dot{\mathbf{r}}) \times \frac{d \mathbf{r}}{d \tilde{s}} \right] \right\} \tag{14}$$

2.2. Equations of Motion

The force balance on the segment of mooring line leads to

$$\frac{d \mathbf{F}_E}{d \tilde{s}} + \mathbf{q}_E = \tilde{m} \ddot{\mathbf{r}} \tag{15}$$

where \mathbf{F}_E is the cross-section internal force (see Figure 1). The balance of moments on the same segment can be expressed as

$$\frac{d \mathbf{r}}{d \tilde{s}} \times \mathbf{F}_E = 0 \tag{16}$$

By inspecting the above equations, one finds that bending and torsional stiffnesses are neglected because only the internal force is considered on the cross-section, i.e., there is no internal cross-sectional moment. Consequently, the rotary inertia terms are not accounted for. Furthermore, the cross-section is assumed to be homogeneous and circular and without shear deformation. Governing equations are treated in the global coordinate system.

Equation (12) contains 2 parallel vectors since the vector product in it equals zero. This fact is used to establish the following relation

$$\mathbf{F}_E = T_E \frac{d \mathbf{r}}{d \tilde{s}} \tag{17}$$

where T_E is a scalar value and it represents the effective tension force [51,52]. By combining Equations (11) and (13), one obtains the equation of motion of the mooring line:

$$\frac{d}{d \tilde{s}} \left(T_E \frac{d \mathbf{r}}{d \tilde{s}} \right) + \mathbf{q}_E = \tilde{m} \ddot{\mathbf{r}} \tag{18}$$

where the first term on the left-hand side represents the geometric stiffness. Detailed derivations of Equations (13) and (14) can be found in [48]. The final form of the motion equation is obtained by using Equations (1)–(9) and (12)–(14) as

$$\frac{d}{d s} \left(\frac{T_E}{1 + \varepsilon} \frac{d \mathbf{r}}{d s} \right) + m \mathbf{g} - \rho A \mathbf{g} + (1 + \varepsilon) \mathbf{q}_H = m \ddot{\mathbf{r}} \tag{19}$$

with

$$\begin{aligned}
 (1 + \varepsilon)\mathbf{q}_H = & -C_A \rho A \frac{1}{(1+\varepsilon)^2} \frac{d\mathbf{r}}{ds} \times \left(\ddot{\mathbf{r}} \times \frac{d\mathbf{r}}{ds} \right) + \\
 & + C_M \rho A \frac{1}{(1+\varepsilon)^2} \frac{d\mathbf{r}}{ds} \times \left(\dot{\mathbf{v}} \times \frac{d\mathbf{r}}{ds} \right) + \\
 & + \frac{1}{2} C_D \rho D \frac{\sqrt{1+\varepsilon}}{(1+\varepsilon)^3} \left\| (\mathbf{v} - \dot{\mathbf{r}}) \times \frac{d\mathbf{r}}{ds} \right\| \left\{ \frac{d\mathbf{r}}{ds} \times \left[(\mathbf{v} - \dot{\mathbf{r}}) \times \frac{d\mathbf{r}}{ds} \right] \right\}
 \end{aligned} \tag{20}$$

2.3. Discretisation of the Motion Equation

Discretisation of the equation of motion is conducted to define a non-linear finite element for solving the dynamics of the entire mooring line. The axial deformation ε in Equation (20) is involved in an inconvenient way. A simplification can be obtained by the use of Taylor series expansion

$$\frac{1}{(1 + \varepsilon)^2} = 1 - 2\varepsilon + 3\varepsilon^2 + O(\varepsilon^3) \tag{21}$$

and

$$\frac{\sqrt{1 + \varepsilon}}{(1 + \varepsilon)^3} = 1 - \frac{5}{2}\varepsilon + \frac{35}{8}\varepsilon^2 + O(\varepsilon^3) \tag{22}$$

Furthermore, the relation between the axial deformation ε and the effective tension force T_E is given in a simplified manner as

$$\varepsilon = \frac{T_E}{AE} \tag{23}$$

where AE is the axial stiffness of the synthetic rope, which can be modelled as a non-linear function dependant on the tension. This simplified expression is valid within the assumption that the Poisson’s ratio for synthetic ropes is 0.5 [44].

By a combination of the above expressions and Equation (20), a form of hydrodynamic loads that is more convenient for discretisation is obtained. It can be written using the index notation as

$$\begin{aligned}
 (1 + \varepsilon)(q_H)_i = & -C_A \rho A \left(1 - \frac{2}{AE} T_E + \frac{3}{(AE)^2} T_E^2 \right) e_{ifg} r'_f e_{gjh} \ddot{r}'_h + \\
 & + C_M \rho A \left(1 - \frac{2}{AE} T_E + \frac{3}{(AE)^2} T_E^2 \right) e_{ifg} r'_f e_{gjh} \dot{v}'_h + \\
 & + \frac{1}{2} C_D \rho D \left(1 - \frac{5}{2AE} T_E + \frac{35}{8(AE)^2} T_E^2 \right) \\
 & \sqrt{[e_{abc}(v_b - \dot{r}_b)r'_c] [e_{ade}(v_d - \dot{r}_d)r'_e] [e_{ifg} r'_f e_{gjh} (v_j - \dot{r}_j)r'_h]}
 \end{aligned} \tag{24}$$

where prime denotes differentiation with respect to s and e_{ijk} is the Levi–Civita symbol. All indices used here are in the range from 1 to 3. The unknown variables T_E and r_i are approximated as

$$r_i(s, t) = A_l(s) U_{il}(t) \tag{25}$$

$$T_E(s, t) = P_m(s) \lambda_m(t) \tag{26}$$

with

$$m = 1, 2, 3; l = 1, \dots, 4 \tag{27}$$

where A_l and P_m are shape functions (i.e., polynomials) defined in the interval $0 \leq s \leq L$, where L is the length of the finite element (see [48]). Unknown node displacements U_{il} and node effective tensions λ_m are expressed as

$$\begin{aligned}
 U_{i1}(t) = r_i(0, t); U_{i2}(t) = r'_i(0, t) \\
 U_{i3}(t) = r_i(L, t); U_{i4}(t) = r'_i(L, t)
 \end{aligned} \tag{28}$$

and

$$\begin{aligned} \lambda_1(t) &= T_E(0, t) \\ \lambda_2(t) &= T_E(L/2, t) \\ \lambda_3(t) &= T_E(L, t) \end{aligned} \tag{29}$$

By above equations, the finite element developed here has 3 nodes, 2 end nodes, and 1 mid-node positioned at $L/2$. Each end node comprises displacements in the sense of 3 translations and 3 rotations in the Cartesian coordinate system and the particular value of the effective tension force as an additional degree of freedom since the tension force is also an unknown value. The mid-node is introduced to give a better approximation of the effective tension over the length of the element so that the mid-node only contains the tension. Overall, the finite element has 15 degrees of freedom, where the only connection nodes are the end nodes, i.e., the mid-node is not a connection node.

The Galerkin method is used for the finite element formulation so that the final form of the discretised motion equation is obtained as

$$\begin{aligned} & \left(M_{ijkl} + M_{ijkl}^{A0} + \lambda_n M_{nijkl}^{A1} + \lambda_n \lambda_m M_{nmijkl}^{A2} \right) \ddot{U}_{jk} + \\ & + \left(K_{nijkl}^{20} + \lambda_m K_{nmijkl}^{21} + \lambda_m \lambda_p K_{nmpijkl}^{22} \right) \lambda_n U_{jk} = F_{il} + F_{il}^{M0} + \lambda_n F_{nil}^{M1} + \lambda_n \lambda_m F_{nmil}^{M2} + \\ & \qquad \qquad \qquad + F_{il}^{D0} + \lambda_n F_{nil}^{D1} + \lambda_n \lambda_m F_{nmil}^{D2} \end{aligned} \tag{30}$$

with

$$M_{ijkl}^{A0} = \int_0^L H_{ijkl} \, ds \tag{31}$$

$$M_{nijkl}^{A1} = - \int_0^L \frac{2P_n}{AE} H_{ijkl} \, ds \tag{32}$$

$$M_{nmijkl}^{A2} = \int_0^L \frac{3P_n P_m}{(AE)^2} H_{ijkl} \, ds \tag{33}$$

$$F_{il}^{M0} = \int_0^L J_{il} \, ds \tag{34}$$

$$F_{nil}^{M1} = - \int_0^L \frac{2P_n}{AE} J_{il} \, ds \tag{35}$$

$$F_{nmil}^{M2} = \int_0^L \frac{3P_n P_m}{(AE)^2} J_{il} \, ds \tag{36}$$

$$F_{il}^{D0} = \int_0^L N_{il} \, ds \tag{37}$$

$$F_{nil}^{D1} = - \int_0^L \frac{5P_n}{2AE} N_{il} \, ds \tag{38}$$

$$F_{nmil}^{D2} = \int_0^L \frac{35P_n P_m}{8(AE)^2} N_{il} \, ds \tag{39}$$

and substitutions

$$H_{ijkl} = (C_A \rho A) A_l e_{ifg} A'_v e_{gjh} A_k A'_z U_{fv} U_{hz} \tag{40}$$

$$J_{il} = (C_M \rho A) A_l e_{ifg} A'_v e_{gjh} A'_z P_q W_{jq} U_{fv} U_{hz} \tag{41}$$

$$N_{il} = \left(\frac{1}{2}C_D\rho D\right)\sqrt{\left[e_{abc}\left(P_qQ_{bq}-A_r\dot{U}_{br}\right)A'_sU_{cs}\right]\left[e_{ade}\left(P_rQ_{dr}-A_t\dot{U}_{dt}\right)A'_uU_{eu}\right]}\cdot\left[A_levfgA'_ve_{gh}\left(P_pQ_{jp}-A_k\dot{U}_{jk}\right)A'_zU_{fv}U_{hz}\right] \tag{42}$$

where Q_{br} and W_{jq} are nodal velocities and accelerations of the surrounding seawater, respectively. It should be noted that all integrals in the above set of equations can be evaluated analytically except for the integrals for the drag forces, i.e., the Equations (37)–(39).

In the discretised equation of motion, M_{ijkl}^{A0} is the added mass matrix (i.e., tensor) of a mooring line. This added mass is derived from the hydrodynamic loads, i.e., from the first term in Equation (8). It is used for the calculation of inertial forces (due to the motions through seawater) by multiplication with the node accelerations \ddot{U}_{jk} (see Equation (30)). The M_{ijkl}^{A0} can be considered as the added mass of a mooring line in the non-extended state when there is no reduction of the mooring line diameter.

M_{nijkl}^{A1} has the origin in the same term in Equation (8) and can be loosely referred to as the added mass. This matrix is a direct consequence of the simplification based on the Taylor series expansion where the inconvenient involvement of the axial deformation ε in hydrodynamic loads is resolved (see Equations (21), (23), and (24)). More precisely, it is the second term of the Taylor series from Equation (20), i.e., -2ε , that causes M_{nijkl}^{A1} to be populated with non-zero elements. The inertial forces are obtained from this matrix by multiplication with the node effective tension λ_n and with \ddot{U}_{jk} (see Equation (30)). In this way, the change of internal forces due to the elongation and the diameter reduction is obtained through the tension λ_n . This change is linearly proportional to λ_n . Thus, M_{nijkl}^{A1} can be comprehended as the linear change coefficients matrix of the added mass.

In an analogous way, M_{nmijkl}^{A2} is the quadratic change coefficients matrix of the added mass since it originates from the quadratic term $3\varepsilon^2$ of the Taylor series in Equation (20). The quadratic influence on the inertial forces can be noticed in Equation (30) where the term is multiplied by $\lambda_n \lambda_m$ besides multiplication by \ddot{U}_{jk} .

Following a similar pattern, F_{il}^{D0} is the node force vector calculated for the non-extended state of the mooring line comprising the drag load part of the hydrodynamic loads, i.e., the second and the third term of Equation (8). F_{nil}^{D1} and F_{nmil}^{D2} are derived from linear and quadratic terms in the Taylor series (see Equation (22)). Thus, F_{nil}^{D1} is the linear change and F_{nmil}^{D2} is the quadratic change matrix of the drag load, which are introduced to incorporate diameter changes and the elongation of the mooring line into the hydrodynamic loads. Finally, the analogy stands for the inertial part of the load, i.e., for F_{il}^{M0} , F_{nil}^{M1} , and F_{nmil}^{M2} .

Other matrices and vectors used in the discretised motion equation in Equation (30) are derived and explained in [48]. In the same paper, an axial elongation condition is presented that is necessary to fully define the mathematical model for solving the mooring line dynamics. In Equation (30), the motion equation is presented with 2 unknowns, the displacements U_{il} and the effective tension λ_m . Consequently, an additional equation is needed, and it is obtained using the axial elongation condition.

3. Case Studies

Within these case studies, the range of axial deformation from 0.0 to 0.3 was observed, which covers the usual deformations of different types of synthetic ropes in use. These are relatively high values of deformations regarding conventional models used in the current practice. The model proposed here was intentionally developed for such deformations since the diameter reduction and its influence on the hydrodynamic reactions are significant at relatively high axial deformations. Currently, there are no available experimental results or full-scale measurements that are focused on this issue in detail that could be used as a base for validations of the proposed model and comparisons with the current practice. Therefore, an alternative approach based on exact analytical expressions was used. The analytical expressions were derived without any dependency with the proposed model to

be used for calculating the inertial and the drag forces. As such, these expressions can be used for independent numerical validations.

To make the derivations of these analytical expressions possible, we considered simple mooring line segments within the case studies, i.e., a straight segment and a curved segment. Both segments had prescribed displacements and were subjected to prescribed fluid velocities and accelerations. Thus, these expressions considered the diameter reduction due to the axial deformation (of observed segments) in the inertial and the drag forces and consequently in the evaluation of the damping and the added mass in an exact analytical way. Finally, these expressions were used to show the achieved improvements of the proposed model over the current practice.

The analytical expressions were not capable of describing the motions of observed segments. As noted, the displacements were prescribed and constant in time. In such circumstances, there is no need for the definition of the boundary conditions. The fluid (i.e., the seawater) velocities and accelerations were also prescribed and constant in time and space. Therefore, the analytical expressions gave the forces for such simplified conditions. For the same simplified conditions, the corresponding forces were calculated with expressions from the proposed model, i.e., from the developed finite element to conduct the numerical validations and to demonstrate archived improvements.

3.1. Straight Segment

To illustrate the effectiveness of the newly developed model, we first observed a straight segment made of synthetic rope. The properties of the rope are listed in Table 1. The configuration of the segment is shown in Figure 3. The segment was positioned in the vertical direction. The self-wet weight of the rope was neglected in this case. Only one finite element was used for the segment with an assumption that the value of the axial deformation was constant over the element length. On the basis of the presented assumptions, we formulated the nodal displacements and the nodal tensions as per Equations (28) and (29), respectively:

$$U_{jk} = \begin{bmatrix} 0 & 0 & 0 & 0 \\ 0 & 0 & 0 & 0 \\ 0 & 1 + \varepsilon & L(1 + \varepsilon) & 1 + \varepsilon \end{bmatrix} \tag{43}$$

and

$$\lambda_n = AE \langle \varepsilon \quad \varepsilon \quad \varepsilon \rangle \tag{44}$$

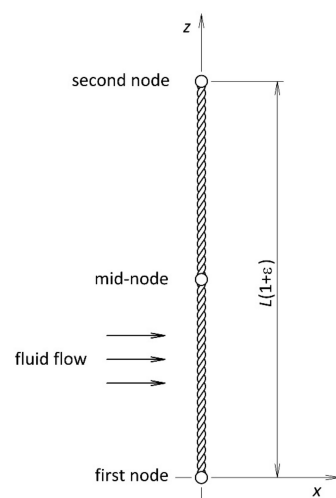


Figure 3. The configuration of the straight segment.

Table 1. Properties of synthetic rope.

Designation	Quantity	Unit
Length, L	10.0	m
Diameter, D	160	mm
Distributed mass, m	17.197	kg/m
Wet weight, q_w	44.102	N/m
Linearised axial stiffness, AE	$1.6812 \cdot 10^8$	N
Added mass coefficient, C_A	1.15	
Inertial coefficient, C_M	2.15	
Drag coefficient, C_D	2.2	

For the evaluation of inertial forces due to the added mass, we assumed a unit lateral acceleration of the segment in the horizontal direction. Similarly, unit velocity of the segment was defined for the calculation of drag forces. In such a simplified case, nodal velocities and accelerations can be expressed as

$$\dot{U}_{il} = \ddot{U}_{il} = \begin{bmatrix} 1 & 0 & 1 & 0 \\ 0 & 0 & 0 & 0 \\ 0 & 0 & 0 & 0 \end{bmatrix} \tag{45}$$

Here, the two tensors for velocities and accelerations had the same quantities but different measuring units, i.e., for the velocities, m/s was used, and for the accelerations, m/s².

Similarly, inertial forces are calculated on the basis of unit acceleration (in the horizontal direction) of the surrounding seawater that is constant over the depth. Drag forces are based on unit velocity. Therefore, the nodal values are formulated (keeping in mind the proper measuring units) as

$$Q_{br} = W_{jq} = \begin{bmatrix} 1 & 1 & 1 \\ 0 & 0 & 0 \\ 0 & 0 & 0 \end{bmatrix} \tag{46}$$

3.1.1. Inertial Forces on the Straight Segment

Calculations of the nodal forces of the observed segment modelled by only one finite element can be conducted by using the already mentioned assumptions and the nodal values defined for the accelerations. Inertial forces due to the added mass, designated as F_{il}^A , are straightforwardly calculated as follows (see Equation (30)):

$$F_{il}^A = \left(M_{ijkl}^{A0} + \lambda_n M_{nijkl}^{A1} + \lambda_n \lambda_m M_{nmijkl}^{A2} \right) \ddot{U}_{jk} \tag{47}$$

The expression above takes into account the diameter change and the elongation of the segment through the newly developed terms M_{nijkl}^{A1} and M_{nmijkl}^{A2} . Without these terms, the evaluation would be conducted in a manner that is done according to the current practice presented in the literature review as follows:

$$F_{il}^{A0} = M_{ijkl}^{A0} \ddot{U}_{jk} \tag{48}$$

In order to illustrate the improvement due to the new model, we next present the results of calculations with and without these members.

Since a simple model is considered here, it is possible to analytically determine nodal inertial forces that can be compared with the new model and models from the current practice. In this way, a quality verification of the new model can be obtained. Using the Morison equation and the assumptions of the simple model used here, one can evaluate nodal inertial force as

$$f^A = - C_A \rho \tilde{A} a \frac{\tilde{L}}{2} \tag{49}$$

where a is the unit horizontal acceleration. \tilde{L} is the extended length of the segment that can be determined as follows (see Equation (5)):

$$\tilde{L} = (1 + \varepsilon)L \tag{50}$$

Only half of the extended segment length is included in Equation (49) because a single node receives only half of the total finite element load. The above expression can be simplified using Equation (7) as

$$f^A = -C_A \rho A a \frac{L}{2} \tag{51}$$

Inertial forces due to the acceleration of the surrounding seawater are calculated as follows (see Equation (30)):

$$F_{il}^M = F_{il}^{M0} + \lambda_n F_{nil}^{M1} + \lambda_n \lambda_m F_{nmil}^{M2} \tag{52}$$

where F_{nil}^{M1} and F_{nmil}^{M2} are the additional terms developed in the new model. The current practice models use only the first member F_{il}^{M0} . Analytical approximation of the nodal forces is derived following the same pattern as for Equation (51):

$$f^M = C_M \rho A a \frac{L}{2} \tag{53}$$

Table 2 presents a comparison between numerical values of the inertial force due to the added mass obtained in different ways. The base for the comparison is the analytically determined force f^A that can be considered as an exact evaluation of this force (see Equation (51)). The table gives values determined in the usual way, by Equation (48), where the nodal inertial force denoted as F_{il}^{A0} is calculated regardless of the segment elongation and the diameter reduction of the rope. The values obtained by the new model, i.e., F_{il}^A expressed by Equation (47), take into account the specifics of synthetic ropes regarding their extensibility. The table also gives the percentage of the relative deviation of the numerical models from the analytical solution in order to present the improvement in accuracy of the new model. Table 3 is formed in an analogous way regarding the inertial force caused by acceleration of the surrounding seawater.

Table 2. Inertial forces on the straight segment due to the added mass.

ε	f^A, N	F_{11}^{A0}, N	F_{11}^A, N	$(F_{11}^{A0} - f^A) / f^A, \%$	$(F_{11}^A - f^A) / f^A, \%$
0.00	-118.5	-118.5	-118.5	0.0	0.0
0.05	-118.5	-130.6	-118.6	10.2	0.1
0.10	-118.5	-143.4	-119.0	21.0	0.4
0.15	-118.5	-156.7	-120.2	32.2	1.5
0.20	-118.5	-170.6	-122.9	44.0	3.7
0.25	-118.5	-185.2	-127.3	56.2	7.4
0.30	-118.5	-200.3	-134.2	69.0	13.2

Table 3. Inertial forces on the straight segment due to the incoming flow.

ε	f^M, N	F_{11}^{M0}, N	F_{11}^M, N	$(F_{11}^{M0} - f^M) / f^M, \%$	$(F_{11}^M - f^M) / f^M, \%$
0.00	221.6	221.5	221.6	0.0	0.0
0.05	221.6	244.3	221.7	10.2	0.1
0.10	221.6	268.1	222.5	21.0	0.4
0.15	221.6	293.0	224.9	32.2	1.5
0.20	221.6	319.0	229.7	44.0	3.7
0.25	221.6	346.2	238.0	56.2	7.4
0.30	221.6	374.4	250.9	69.0	13.2

Tables 2 and 3 contain the same relative deviations of the numerical models from the exact analytical solutions. The inertial forces are calculated for the simplified straight segment. Such a set-up is the major cause of this. The mathematical models used are very similar in general, but for this simplified set-up are the same. The origins of these models are on the right side of Equation (20) in the first and the second row. The cause can also be found in the definition of the applied accelerations. In Table 2, where the inertial forces due to the added mass are shown, it is assumed that the segment is in motion with the unit horizontal acceleration immersed in the still seawater. Table 3, with the inertial forces due to the incoming flow, assumes that the segment is fixed while the incoming flow has the unit horizontal acceleration.

3.1.2. Drag Forces on the Straight Segment

The total drag forces F_{ij}^D are also evaluated using Equation (30) as

$$F_{ij}^D = F_{ij}^{D0} + \lambda_n F_{nil}^{D1} + \lambda_m \lambda_n F_{nmil}^{D2} \tag{54}$$

where F_{nil}^{D1} and F_{nmil}^{D2} are the new terms, whereas F_{ij}^{D0} is the term used in the current practice.

For the straight segment, it is possible to formulate analytical expression for the nodal drag forces as

$$f^D = \frac{1}{2} \rho C_D \tilde{D} |v| v \frac{L}{2} \tag{55}$$

Or by using Equations (9) and (50):

$$f^D = \frac{1}{2} \rho C_D D |v| v \frac{L}{2} \sqrt{1 + \varepsilon} \tag{56}$$

where v is unit horizontal velocity and $| \cdot |$ denotes the absolute value of a number.

Tables 4 and 5 provide comparisons of drag forces as well as their deviation from the analytical values. Table 4 considers the segment motions, whereas Table 5 considers the incoming fluid flow. The relative deviations of the numerical models from the exact analytical solutions in Tables 4 and 5 are the same for the same values of the axial deformations. The cause of this is in the simplified set-up used in these case studies. Moreover, the same mathematical model is used for the calculation of the observed drag forces, which has the origin in the last row of the right side of Equation (20). Here, it should be kept in mind that Table 4 presents the drag forces due to the segment motions with the unit horizontal velocity, while Table 5 presents the same type of forces but for the fixed segments in the incoming flow with the unit horizontal velocity.

Table 4. Drag forces on the straight segment due to the segment motion.

ε	f^D, N	F_{11}^{D0}, N	F_{11}^D, N	$(F_{11}^{D0} - f^D) / f^D, \%$	$(F_{11}^D - f^D) / f^D, \%$
0.00	-902.0	-902.0	-902.0	0.0	0.0
0.05	-924.3	-1044.2	-925.1	13.0	0.1
0.10	-946.0	-1200.6	-953.0	26.9	0.7
0.15	-967.3	-1371.8	-992.4	41.8	2.6
0.20	-988.1	-1558.7	-1052.1	57.7	6.5
0.25	-1008.4	-1761.7	-1142.4	74.7	13.3
0.30	-1028.4	-1981.7	-1275.7	92.7	24.0

Table 5. Drag forces on the straight segment sea due to the incoming flow.

ϵ	f^D, N	F_{11}^{D0}, N	F_{11}^D, N	$(F_{11}^{D0} - f^D) / f^D, \%$	$(F_{11}^D - f^D) / f^D, \%$
0.00	902.0	902.0	902.0	0.0	0.0
0.05	924.3	1044.2	925.1	13.0	0.1
0.10	946.0	1200.6	953.0	26.9	0.7
0.15	967.3	1371.8	992.4	41.8	2.6
0.20	988.1	1558.7	1052.1	57.7	6.5
0.25	1008.4	1761.7	1142.4	74.7	13.3
0.30	1028.4	1981.7	1275.7	92.7	24.0

3.2. Curved Segment

To further illustrate the effectiveness of the new model, we next considered a curved mooring line. The same properties of the rope were used as before. Moreover, the same values of horizontal velocity and accelerations were applied. The initial length of the segment was the same as for the straight segment. The configuration of the curved segment is shown in Figure 4. Again, only one finite element was used with constant values of the axial deformation over the element length. Appropriate nodal displacements needed to be evaluated in the first step, on the basis of the extended length of the segment and a given horizontal deflection. The horizontal deflection was assumed to be 20% of the extended length of the segment given for the mid-node. Calculation of such nodal displacements can only be performed numerically (in this case, using the Newton–Raphson method). Within the method, an effort was made to ensure that the deflection line had as constant a radius of curvature as possible, i.e., the deflection line resembled a circular arc.

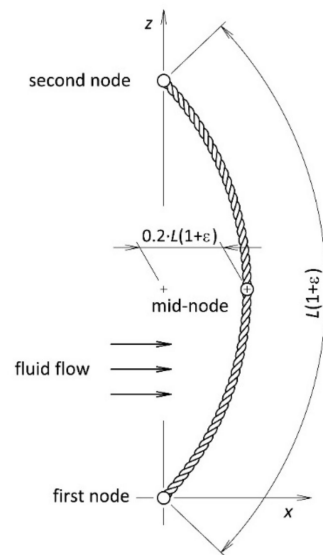


Figure 4. The configuration of the curved segment.

3.2.1. Inertial Forces on the Curved Segment

Once the nodal displacements of the curved segment were determined, it was possible to calculate the total inertial forces due to the added mass in an analytical way (in the horizontal direction). The Morrison equation was again used to obtain a simple expression

$$f^A = - C_A \rho \tilde{A} a \int_0^{\tilde{L}/2} \left(\frac{d r_3}{d \tilde{s}} \right)^2 d \tilde{s} \tag{57}$$

or by using Equations (5) and (7):

$$f^A = - \frac{C_A \rho A a}{(1 + \varepsilon)^2} \int_0^{L/2} \left(\frac{d r_3}{d s} \right)^2 d s \tag{58}$$

In the above expression, the integral can be solved analytically since the r_3 is a third-order polynomial (see Equation (25)). The integration was carried out over the half-length of the segment, since it was assumed again that a single node receives only half of the total finite element load. In an analogue way, inertial forces of the surrounding seawater can be approximated as

$$f^M = \frac{C_M \rho A a}{(1 + \varepsilon)^2} \int_0^{L/2} \left(\frac{d r_3}{d s} \right)^2 d s \tag{59}$$

The relative deviation of the inertial forces (for the curved segment) from analytical values is shown in Figure 5, where current models are compared with the new model.

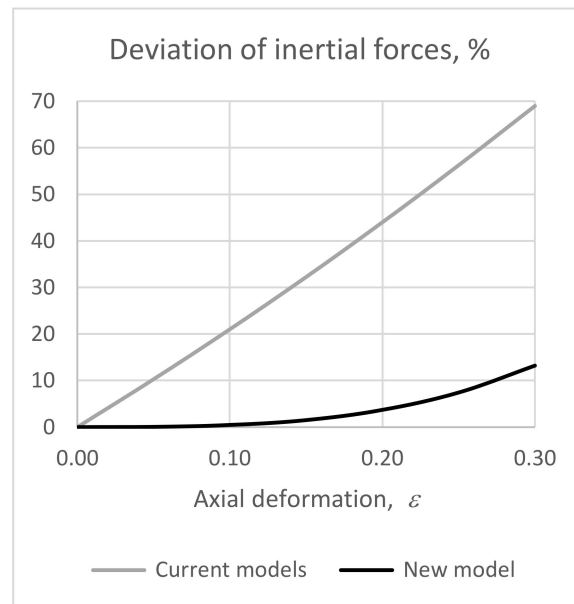


Figure 5. Deviation of inertial forces for the curved segment.

3.2.2. Drag Forces on the Curved Segment

The expression for the nodal drag forces can be formulated as

$$f^D = \frac{1}{2} \rho C_D \tilde{D} |v|v \int_0^{\tilde{L}/2} \left(\frac{d r_3}{d \tilde{s}} \right)^3 d \tilde{s} \tag{60}$$

and with the use of Equations (5) and (9):

$$f^D = \frac{1}{2} \rho C_D D |v|v \frac{\sqrt{1 + \varepsilon}}{(1 + \varepsilon)^3} \int_0^{L/2} \left(\frac{d r_3}{d s} \right)^3 d s \tag{61}$$

where the integral can be solved analytically. The deviation of drag forces is presented in Figure 6.

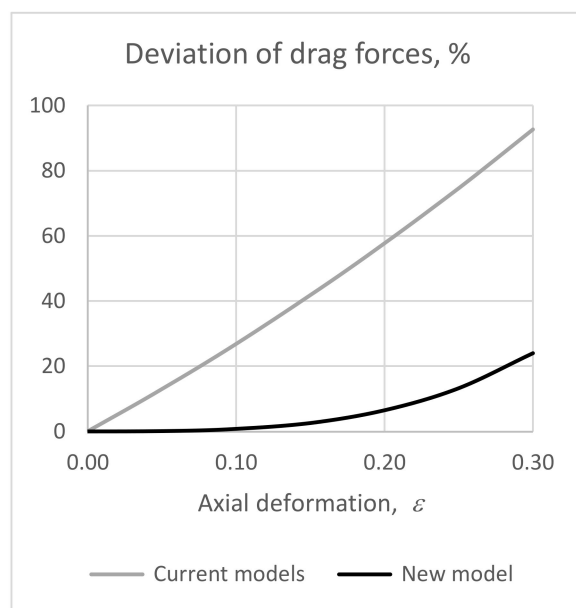


Figure 6. Deviation of drag forces for the curved segment.

4. Conclusions

This study presents a new finite element intended for modelling of mooring lines made of synthetic fibre ropes. The specifics of the kind of rope was considered in the calculation of damping and added mass. New terms in the finite element formulation were developed and added in order to capture the influence of large values of axial deformation of a mooring line, and consequently the effect of the outer diameter reduction in calculation of hydrodynamic reactions. The new terms in the formulation can be comprehended as a linear and a quadratic change of hydrodynamic reactions due to the deformations of synthetic ropes. The current practice does not consider these deformations and therefore overestimates forces due to damping and the added mass.

In order to present the effectiveness of the new model, we studied a set of simple mooring lines, i.e., mooring line segments, namely, a straight and a curved segment with predefined deflections. For these simple segments, analytical formulas were derived that were exact expressions for the hydrodynamic reactions. These analytical expressions were used as a base for comparison of the current practice model and the new model.

Damping forces due to a prescribed motion of a segment and due to an incoming flow were evaluated. The range of the axial deformation from 0 to 0.3 was considered. Comparisons revealed that the current practice significantly overestimated damping forces. For the axial deformation of 0.2, this overestimation was approximately 58% in comparison to the analytical results. The new model had a much better correlation with the analytical calculations, and the overestimation was only 6.5%.

Inertial forces caused by prescribed accelerations were also calculated. The same range of axial deformations 0 to 0.3 was considered. The current practice models overestimated these forces by approximately 44% for both segments. The new model once again achieved significantly better correlation with the analytical calculations. The overestimation in this case was 3.7%, which clearly demonstrated the effectiveness of the new model.

In general, the new model reduced the overestimation of the hydrodynamic reactions by one order of magnitude for the set of a simple case studies considered. Nevertheless, there was room for improvement. This was because with axial deformations approximately above 0.17, the overestimates of the new model were above the usual engineering acceptable error of to 2%. Moreover, the new model is numerically more demanding and should be tested within a coupled dynamic analysis of a mooring system and a moored vessel since the new members in the finite element formulation are the tensors up to the sixth order. This can be a direction for future investigations.

Author Contributions: Conceptualisation, I.Ć.; methodology, I.Ć. and N.A.; software, I.Ć., V.S., and S.R.; formal analysis, I.Ć. and N.A.; investigation, V.S. and S.R.; resources, V.S.; writing—original draft preparation, I.Ć.; writing—review and editing, N.A., V.S., and S.R. All authors have read and agreed to the published version of the manuscript.

Funding: This research received no external funding.

Institutional Review Board Statement: Not applicable.

Informed Consent Statement: Not applicable.

Acknowledgments: The Croatian Science Foundation HRZZ-IP-2016-06-2017 (WESLO) support is gratefully acknowledged. This work was supported by Croatian Science Foundation under the project IP-2019-04-5402.

Conflicts of Interest: The authors declare no conflict of interest.

References

1. Wang, S.; Xu, S.; Xiang, G.; Soares, C.G. An overview of synthetic mooring cables in marine applications. In *Advances in Renewable Energies Offshore—Guedes Soares*; Taylor & Francis Group: London, UK, 2019.
2. Xu, S.; Wang, S.; Soares, C.G. Review of mooring design for floating wave energy converters. *Renew. Sustain. Energ. Rev.* **2019**, *111*, 595–621. [[CrossRef](#)]
3. Sudaia, D.P.; Bastos, M.B.; Fernandes, E.B.; Nascimento, C.R.; Pacheco, E.B.A.V.; da Silva, A.L.N. Sustainable recycling of mooring ropes from decommissioned offshore platforms. *Mar. Pollut. Bull.* **2018**, *135*, 357–360. [[CrossRef](#)]
4. Apolonia, M.; Simas, T. Life Cycle Assessment of an Oscillating Wave Surge Energy Converter. *J. Mar. Sci. Eng.* **2021**, *9*, 206. [[CrossRef](#)]
5. Webster, W.C. Mooring-induced damping. *Ocean Eng.* **1995**, *22*, 571–591. [[CrossRef](#)]
6. Balzola, R. Mooring Line Damping in Very Large Water Depths. Master's Thesis, The Department of Ocean Engineering, Massachusetts Institute of Technology, Cambridge, MA, USA, 1999.
7. Zhao, Z.; Li, X.; Wang, W.; Shi, W. Analysis of Dynamic Characteristics of an Ultra-Large Semi-Submersible Floating Wind Turbine. *J. Mar. Sci. Eng.* **2019**, *7*, 169. [[CrossRef](#)]
8. Huse, E.; Matsumoto, K. Mooring line damping due to first and second order vessel motion. In Proceedings of the 21st Offshore Technology Conference, Paper 6137, Houston, TX, USA, 1–4 May 1989.
9. Nishimoto, K.; Kaster, F.; Masetti, I.Q.; Matsuura, J.; Aranha, J.A.P. Full scale decay test of a tanker: Field data and theoretical analysis. *Ocean Eng.* **1999**, *26*, 125–145. [[CrossRef](#)]
10. Fan, T.; Qiao, D.; Ou, J. Innovative approach to design truncated mooring system based on static and damping equivalent. *Ships Offshore Struct.* **2014**, *9*, 557–568. [[CrossRef](#)]
11. Ma, G.; Wang, H.; Sun, L.; Jiang, Y. Dynamic truncation method for mooring lines with tension estimation combined in the time and frequency domains. *Ships Offshore Struct.* **2018**, *13*, 310–319. [[CrossRef](#)]
12. Fan, T.; Ren, N.; Cheng, Y.; Chen, C.; Ou, J. Applicability analysis of truncated mooring system based on static and damping equivalence. *Ocean Eng.* **2018**, *147*, 458–475. [[CrossRef](#)]
13. Sarkar, A.; Eatock Taylor, R. Effects of mooring line drag damping on response statistics of vessels excited by first and second-order wave forces. *Ocean Eng.* **2000**, *27*, 667–686. [[CrossRef](#)]
14. Yang, Y.; Chen, J.X.; Huang, S. Mooring line damping due to low-frequency superimposed with wave-frequency random line top end motion. *Ocean Eng.* **2016**, *112*, 243–252. [[CrossRef](#)]
15. Xu, S.; Ji, C.; Soares, C.G. Experimental study on taut and hybrid moorings damping and their relation with system dynamics. *Ocean Eng.* **2018**, *154*, 322–340. [[CrossRef](#)]
16. Xiong, L.; Lu, W.; Li, X.; Guo, X. Estimation of damping induced by taut mooring lines. *Int. J. Nav. Archit. Ocean Eng.* **2020**, *12*, 810–818. [[CrossRef](#)]
17. Nielsen, F.G.; Bindingbø, A.U. Extreme loads in taut mooring lines and mooring line induced damping: An asymptotic approach. *Appl. Ocean Res.* **2000**, *22*, 103–118. [[CrossRef](#)]
18. Ali, M.O.A.; Ja'e, I.A.; Hwa, M.G.Z. Effects of water depth, mooring line diameter and hydrodynamic coefficients on the behaviour of deepwater FPSOs. *Ain Shams Eng. J.* **2020**, *11*, 727–739.
19. Johanning, L.; Smith, G.H.; Wolfram, J. Measurements of static and dynamic mooring line damping and their importance for floating WEC devices. *Ocean Eng.* **2007**, *34*, 1918–1934. [[CrossRef](#)]
20. Karimirad, M. Modeling aspects of a floating wind turbine for coupled wave-wind-induced dynamic analyses. *Renew. Energ.* **2013**, *53*, 299–305. [[CrossRef](#)]
21. Robertson, A.; Jonkman, J. Annex 30—Task Extension Proposal, 2019–2022 Offshore Code Comparison Collaboration, Continued, with Correlation, and unCertainty (OC6) 1 Scope, 2019–2022. 2019. Available online: <https://a2e.energy.gov/projects/oc6/documents/Task%2030%20Extension%20Proposal%202019-2022%20ver.2.pdf> (accessed on 1 June 2020).

22. Trubat, P.; Molins, C.; Gironella, X. Wave hydrodynamic forces over mooring lines on floating offshore wind turbines. *Ocean Eng.* **2020**, *195*, 106730. [\[CrossRef\]](#)
23. Chen, C.-T.; Lee, J.-F.; Lo, C.-H. Mooring Drag Effects in Interaction Problems of Waves and Moored Underwater Floating Structures. *J. Mar. Sci. Eng.* **2020**, *8*, 146. [\[CrossRef\]](#)
24. Tahar, A.; Kim, M.H. Hull/mooring/riser coupled dynamic analysis and sensitivity study of a tanker-based FPSO. *Appl. Ocean Res.* **2003**, *25*, 367–382. [\[CrossRef\]](#)
25. Tahar, A.; Kim, M.H. Coupled-dynamic analysis of floating structures with polyester mooring lines. *Ocean Eng.* **2008**, *35*, 1676–1685. [\[CrossRef\]](#)
26. Wiegard, B.; Radtke, L.; König, M.; Abdel-Maksoud, M.; Düster, A. Simulation of the fluid-structure interaction of a floating wind turbine. *Ships Offshore Struct.* **2019**, *14*, 207–218. [\[CrossRef\]](#)
27. Wang, Y. Efficient computational method for the dynamic responses of a floating wind turbine. *Ships Offshore Struct.* **2020**, *15*, 269–279. [\[CrossRef\]](#)
28. Yang, H.; Zhao, Y.-P.; Bi, C.-W.; Cui, Y. Numerical Study on Hydrodynamic Responses of Floating Rope Enclosure in Waves and Currents. *J. Mar. Sci. Eng.* **2020**, *8*, 82. [\[CrossRef\]](#)
29. Vendhan, C.P. Coupled dynamics of deepwater structures—Issues and challenges. *Ships Offshore Struct.* **2019**, *14*, 343–353. [\[CrossRef\]](#)
30. Moura Paredes, G.; Eskilsson, C.; Engsig-Karup, A.P. Uncertainty Quantification in Mooring Cable Dynamics Using Polynomial Chaos Expansions. *J. Mar. Sci. Eng.* **2020**, *8*, 162. [\[CrossRef\]](#)
31. Hermawan, Y.A.; Furukawa, Y. Coupled three-dimensional dynamics model of multi-component mooring line for motion analysis of floating offshore structure. *Ocean Eng.* **2020**, *200*, 106928. [\[CrossRef\]](#)
32. Xu, S.; Soares, C.G. Dynamics of an ultra-deepwater mooring line with embedded chain segment. *Mar. Struct.* **2020**, *72*, 102747. [\[CrossRef\]](#)
33. Domínguez, J.M.; Crespo, A.J.C.; Hall, M.; Altomare, C.; Wu, M.; Stratigaki, V.; Troch, P.; Cappietti, L.; Gómez-Gesteira, M. SPH simulation of floating structures with moorings. *Coast. Eng.* **2019**, *153*, 103560. [\[CrossRef\]](#)
34. Cui, J.; Li, Q.; Cheng, Y.; Ji, C.Y.; Deng, X.K. Addition of dynamic mooring line force based on lumped-mass method in SPH. *Ocean Eng.* **2019**, *182*, 90–101. [\[CrossRef\]](#)
35. Cerveira, F.; Fonseca, N.; Pascoal, R. Mooring system influence on the efficiency of wave energy converters. *Int. J. Mar. Energy* **2013**, *3–4*, 65–81. [\[CrossRef\]](#)
36. Chen, L.; Basu, B.; Nielsen, S.R.K. A coupled finite difference mooring dynamics model for floating offshore wind turbine analysis. *Ocean Eng.* **2018**, *162*, 304–315. [\[CrossRef\]](#)
37. Lee, J.F.; Tu, L.F. Finite element modeling of a single-point multi-segment mooring in water waves. *Ocean Eng.* **2018**, *160*, 461–470. [\[CrossRef\]](#)
38. Cheng, Y.; Ji, C.; Zhai, G.; Oleg, G. Nonlinear analysis for ship-generated waves interaction with mooring line/riser systems. *Mar. Struct.* **2018**, *59*, 1–24. [\[CrossRef\]](#)
39. Lee, H.W.; Roh, M.I.; Ham, S.H.; Ku, N.K. Coupled analysis method of a mooring system and a floating crane based on flexible multibody dynamics considering contact with the seabed. *Ocean Eng.* **2018**, *163*, 555–569. [\[CrossRef\]](#)
40. Jin, C.; Bakti, F.P.; Kim, M.H. Multi-floater-mooring coupled time-domain hydro-elastic analysis in regular and irregular waves. *Appl. Ocean Res.* **2020**, *101*, 102276. [\[CrossRef\]](#)
41. Eidsvik, O.A.N.; Schjølberg, I. Finite element cable-model for Remotely Operated Vehicles (ROVs) by application of beam theory. *Ocean Eng.* **2018**, *163*, 322–336. [\[CrossRef\]](#)
42. Htun, T.Z.; Suzuki, H.; Garcia-Vallejo, D. Dynamic modeling of a radially multilayered tether cable for a remotely-operated underwater vehicle (ROV) based on the absolute nodal coordinate formulation (ANCF). *Mech. Mach. Theory* **2020**, *153*, 103961. [\[CrossRef\]](#)
43. Khalid, F.; Davies, P.; Halswell, P.; Lacotte, N.; Thies, P.R.; Johanning, L. Evaluating Mooring Line Test Procedures through the Application of a Round Robin Test Approach. *J. Mar. Sci. Eng.* **2020**, *8*, 436. [\[CrossRef\]](#)
44. Tjavaras, A.A.; Zhu, Q.; Liu, Y.; Triantafyllou, M.S.; Yue, D.K.P. The mechanics of highly-extensible cables. *J. Sound Vib.* **1998**, *213*, 709–737. [\[CrossRef\]](#)
45. Vu, M.T.; Choi, H.S.; Kang, J.; Ji, D.H.; Jeong, S.K. A study on hovering motion of the underwater vehicle with umbilical cable. *Ocean Eng.* **2017**, *135*, 137–157.
46. Chen, L.; Basu, B.; Nielsen, S.R.K. Nonlinear periodic response analysis of mooring cables using harmonic balance method. *J. Sound Vib.* **2019**, *438*, 402–418. [\[CrossRef\]](#)
47. Palm, J.; Eskilsson, C. Influence of Bending Stiffness on Snap Loads in Marine Cables: A Study Using a High-Order Discontinuous Galerkin Method. *J. Mar. Sci. Eng.* **2020**, *8*, 795. [\[CrossRef\]](#)
48. Čatipović, I.; Čorić, V.; Radanović, J. An improved stiffness model for polyester mooring lines. *Brodogradnja* **2011**, *62*, 235–248.
49. Čatipović, I.; Čorić, V.; Vukčević, V. Dynamics of FPSO with Polyester Mooring Lines. In Proceedings of the 22nd International Offshore and Polar Engineering Conference, Rhodes, Greece, 17–22 June 2012.
50. Lin, Z.; Sayer, P. An enhanced stiffness model for elastic lines and its application to the analysis of a moored floating offshore wind turbine. *Ocean Eng.* **2015**, *109*, 444–453. [\[CrossRef\]](#)

51. Sparks, C.P. *Fundamentals of Marine Riser Mechanics—Basic Principles and Simplified Analyses*; PennWell: Tulsa, OK, USA, 2007.
52. *API RP 16Q. Recommended Practice for Design, Selection, Operation and Maintenance of Marine Drilling Riser Systems*; American Petroleum Institute: Washington, DC, USA, 1993.